Original research

Chromatin state dynamics confers specific therapeutic strategies in enhancer subtypes of colorectal cancer

Elias Orouji ,[1] Ayush T Raman ,[1,2,3] Anand K Singh,[1] Alexey Sorokin,[4] Emre Arslan ,[1] Archit K Ghosh,[1,5] Jonathan Schulz,[1,5] Christopher Terranova,[1] Shan Jiang,[1] Ming Tang,[1] Mayinuer Maitituoheti,[1] Scot C Callahan,[1] Praveen Barrodia,[1] Katarzyna Tomczak,[1] Yingda Jiang,[1,5] Zhiqin Jiang,[4] Jennifer S Davis,[4] Sukhen Ghosh,[6] Hey Min Lee,[4,5] Laura Reyes-Uribe,[7] Kyle Chang,[7] Yusha Liu,[8] Huiqin Chen,[4] Ali Azhdarinia,[6] Jeffrey Morris,[9] Eduardo Vilar ,[5,7] Kendra S Carmon,[5,6] Scott E Kopetz,[4,5] Kunal Rai [1,3,5]

► Additional online supplemental material is published online only. To view, please visit the journal online (http://dx.doi.org/10.1136/gutjnl-2020-322835).

For numbered affiliations see end of article.

Correspondence to
Dr Kunal Rai, Department of Genomic Medicine, University of Texas MD Anderson Cancer Center, Houston, TX 77054, USA; krai@mdanderson.org

EO, ATR and AKS contributed equally.

Received 17 August 2020
Accepted 14 May 2021

To cite: Orouji E, Raman AT, Singh AK, *et al*. *Gut* Epub ahead of print: [*please include* Day Month Year]. doi:10.1136/gutjnl-2020-322835

ABSTRACT

Objective Enhancer aberrations are beginning to emerge as a key epigenetic feature of colorectal cancers (CRC), however, a comprehensive knowledge of chromatin state patterns in tumour progression, heterogeneity of these patterns and imparted therapeutic opportunities remain poorly described.

Design We performed comprehensive epigenomic characterisation by mapping 222 chromatin profiles from 69 samples (33 colorectal adenocarcinomas, 4 adenomas, 21 matched normal tissues and 11 colon cancer cell lines) for six histone modification marks: H3K4me3 for Pol II-bound and CpG-rich promoters, H3K4me1 for poised enhancers, H3K27ac for enhancers and transcriptionally active promoters, H3K79me2 for transcribed regions, H3K27me3 for polycomb repressed regions and H3K9me3 for heterochromatin.

Results We demonstrate that H3K27ac-marked active enhancer state could distinguish between different stages of CRC progression. By epigenomic editing, we present evidence that gains of tumour-specific enhancers for crucial oncogenes, such as *ASCL2* and *FZD10,* was required for excessive proliferation. Consistently, combination of MEK plus bromodomain inhibition was found to have synergistic effects in CRC patient-derived xenograft models. Probing intertumour heterogeneity, we identified four distinct enhancer subtypes (EPIgenome-based Classification, EpiC), three of which correlate well with previously defined transcriptomic subtypes (consensus molecular subtypes, CMSs). Importantly, CMS2 can be divided into two EpiC subgroups with significant survival differences. Leveraging such correlation, we devised a combinatorial therapeutic strategy of enhancer-blocking bromodomain inhibitors with pathway-specific inhibitors (PARPi, EGFRi, TGFβi, mTORi and SRCi) for EpiC groups.

Conclusion Our data suggest that the dynamics of active enhancer underlies CRC progression and the patient-specific enhancer patterns can be leveraged for precision combination therapy.

Significance of this study

What is already known on this subject?

► Chromatin deregulation is an emerging hallmark of cancer. Recent studies have suggested aberrations in enhancer elements in colorectal cancer. However, if and how patient-specific enhancer features could be used for precision medicine is not well understood.

What are the new findings?

► By comprehensive epigenome profiling, we show chromatin state evolution during tumourigenesis, define patient subgroups with different enhancer landscape and identify therapeutic strategies in these epigenetic subgroups.

How might it impact on clinical practice in the foreseeable future?

► Along the theme of personalised medicine, we identify therapeutic strategies for each of these enhancer subgroups which are based on combination of bromodomain inhibitors (BRDi) and a targeted therapy. We demonstrate MEKi plus BRDi as a general therapeutic strategy in colorectal cancer.

INTRODUCTION

Colorectal cancer (CRC) is the third most common cancer in the world. Most cases of CRC originate from premalignant lesions, mainly adenomas, which can progress into malignant adenocarcinomas.[1] Genomic alterations in colorectal adenocarcinomas frequently occur in *APC* (83%), *TP53* (60%), *KRAS* (43%) and *BRAF* (10%) genes.[2–6] However, targeted therapy for these mutational subgroups is not well established. This calls for a comprehensive approach to identify unique signatures derived from various molecular characteristics of tumours including genomic and epigenomic components which, along with clinical features, can be used to introduce clinically feasible targeted therapeutic strategies.

One such effort toward precision therapy was led by the CRC subtyping consortium, which identified four consensus molecular subtypes

(CMSs) with distinct activation patterns of specific oncogenic signalling pathways using gene expression datasets.[3] Briefly, these transcriptomic subgroups include the immune subtype (CMS1), canonical subtype (CMS2), metabolic subtype (CMS3) and mesenchymal subtype (CMS4).[3] Although distal *cis* regulatory elements are known to play a central role in controlling transcription patterns, the bona fide contributions of these elements in defining CMSs are not understood. Importantly, epigenetic processes are reversible and can provide actionable targets for therapeutic development, such as bromodomain inhibitors (BRDi) that target super-enhancer elements (SE).[7] The benefits of targeting the CRC epigenome have already been demonstrated by associations of the CpG island methylator phenotype with BRAF mutations, for which efforts are underway to devise combinatorial strategies targeting methylation and the BRAF oncogene.[3] Consistent with this finding, we and others have provided evidence that epigenomic alterations at the level of DNA methylation play crucial roles in CRC initiation[8] and oncogenic function.[9]

While several studies have profiled enhancer elements in CRC cell lines and few patient samples,[10–13] the enhancer aberrations derived from a relatively larger number of primary untreated patient samples will be highly useful in defining the heterogeneity of the enhancer patterns between patients for precision therapy. Furthermore, a comprehensive understanding of other chromatin state alterations and their functional contribution to tumour progression is mostly lacking. Therefore, it is of immense importance to define the relationship between chromatin aberrations and genomic and transcriptomic features in tumours.

METHODS

Details of all methods are provided in the online supplemental material.

Ethics approval

Not applicable.

RESULTS

To characterise the epigenomic makeup of CRC, we first generated chromatin immunoprecipitation followed by massive parallel sequencing (ChIP-seq)-based profiles for six histone marks including H3K4me1 and H3K27ac, associated with enhancers and transcriptionally active promoters; H3K4me3, associated with PolII-bound and CpG-rich promoters; H3K79me2, associated with transcribed regions; H3K9me3, associated with heterochromatin regions; and H3K27me3, associated with Polycomb repression in a total of 16 CRCs and 17 matching adjacent normal colonic mucosa samples (online supplemental table S1). With the use of the ChromHMM algorithm,[14] we trained a 10-state, 12-state and 15-state model (for samples having all the six marks; online supplemental table S1) consisting of combinatorial patterns of specific histone modifications known as chromatin states, which are linked with the transcriptional output of the associated genomic loci and regulate the recruitment of various components of the transcriptional machinery. We chose a 10-state model for in-depth investigation because it represented biologically interpretable combinatorial patterns that were not repetitive or ambiguous (figure 1A and online supplemental figure S1A). We annotated these chromatin states based on the content of each state and its average relative distribution around known genomic features (online supplemental figure S1B). To define the chromatin states that best differentiate between normal and tumours, we developed a statistical approach, termed ChromXplorer (see the Methods section; online supplemental figure S1C), that uses the ChromDiff[15] framework for all genomic loci instead of a gene-centric approach. The ChromXplorer-based dimensionality reduction approach showed the 'active enhancer' state, but not others, to be the most discriminatory state in all three investigated models (figure 1B and online supplemental figure S1D–F). Analysis of singular histone marks indicated that the active enhancer mark, defined by H3K27ac, also led to clustering of the samples according to their phenotype (online supplemental figure S2A), whereas some of the other histone marks such as H3K79me2, H3K9me3 and H3K27me3 showed weaker clustering patterns due to variations among tumour samples (online supplemental figure S2A), suggesting *de novo* gain or loss of H3K27ac patterns as an important distinguishing feature of CRC.

In light of this, we expanded the cohort by profiling the H3K27ac mark in additional colorectal tumours (n=17), adenomas (n=4), normal crypts (n=4) and cancer cell lines (n=11) to characterise the enhancer patterns through the various stages of progression. Interestingly, distinct enhancer patterns appeared to define each progression stage, suggesting that these enhancer patterns may evolve as the disease progresses (figure 1C). Furthermore, the established CRC cell lines formed a separate cluster with three cell lines that partially overlapped with colorectal adenocarcinoma tumours (figure 1C). Similarly, computation of correlation matrix identified a higher similarity within normal samples as opposed to tumour samples which segregated into two subgroups, indicative of greater heterogeneity between adenocarcinoma specimens (online supplemental figure S2B).

To identify recurrent cancer-specific peaks, shared H3K27ac peaks in all tumour samples were summed up and overlapped with shared normal or shared adenoma enhancers. Our analysis identified 32176 tumour-specific (T) enhancers, 12822 normal-specific (N) enhancers, and 4998 adenoma-specific (A) enhancers (figure 1D). Notably, 5759 enhancers were present in both adenomas and adenocarcinomas, but not in normal tissue, whereas a much higher number (32176) were specific to adenocarcinomas only, thereby, suggesting that several enhancers are gained in *de novo* manner in the adenocarcinoma stage. Furthermore, the average intensity of enhancer peaks was found to progressively increase in adenomas and colorectal tumours (online supplemental figure S2C). Similar to typical enhancers, we found SE, that are thought to promote oncogene expression, to be upregulated in adenocarcinomas (figure 1E). We identified 886 adenocarcinoma-specific, 93 adenoma-specific and 193 shared super enhancers between adenomas and adenocarcinomas using ROSE algorithm[16] (figure 1E).

Active enhancers specific to each disease progression stage marked important driver genes that were identified based on the presence of enhancers in their proximal regulatory regions as previously defined[17 18] (figure 1F and online supplemental table S2). For example, regulators and mediators of the cell cycle, DNA damage, stress and cytokine and metabolism harboured gains in a tumour-specific manner. Conversely, enhancers for regulators of T-cell differentiation, MHC class II antigen presentation, vitamin A metabolism, chemokine signalling and focal adhesion, among others, were specifically present only in normal tissues and were lost during progression. Enhancers common to premalignant adenomas and tumours were enriched around regulators of cell fate, collagen degradation, metabolic transport and wingless/integrated (WNT) signalling (figure 1F). We noted that the enrichment of enhancers/super enhancers in

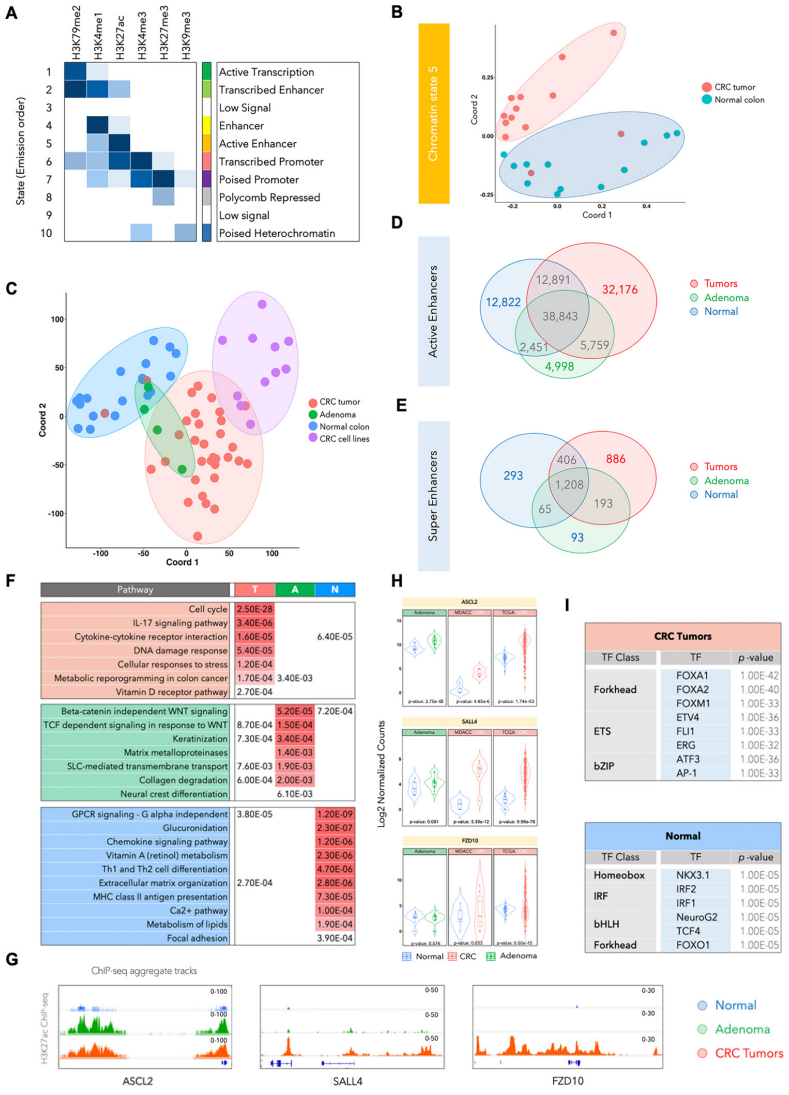

Figure 1 H3K27ac-identified global enhancer pattern could differentiate colorectal cancer (CRC) from normal colon. (A) Emission probabilities of ChromHMM-based 10-chromatin state calls, which is based on the global distribution of combinatorial patterns of 6 histone marks (H3K4me1, H3K27ac, H3K4me3, H3K27me3, H3K79me2 and H3K9me3) from 13 adenocarcinomas and 12 adjacent normal tissues. Each row is representative of a combinatorial chromatin state pattern, which is annotated on the right based on the constituent histone mark and neighbourhood plot (online supplemental figure S1B). Columns represent each histone mark. Colours represent the frequency of occurrence of that mark in the corresponding chromatin state on a scale of 0 (white) to 1 (blue). (B) Multidimensional scaling (MDS) plot for chromatin state five between normal tissues (blue) and adenocarcinoma samples (red). (C) MDS plot for global H3K27ac patterns in the adenomas (A), adenocarcinomas (T), adjacent normal colon (N) and cancer cell lines. Adenoma samples are spread over normal and tumour samples and cannot be distinguished with use of H3K27ac. Red, green, blue and purple colours were used for tumour, adenoma, normal colon and CRC cell lines, respectively. (D) Venn diagram showing overlaps between total number of H3K27ac-defined active enhancer peaks in normal samples (blue), adenomas (green) and CRC tumours (red). (E) Venn diagram showing overlaps between total number of super-enhancer peaks (called using rose) in normal samples (blue), adenomas (green) and CRC tumours (red). (F) List of significantly enriched pathways in genes targeted by enhancers specific to CRC tumours (T), adenomas (A) and normal colon tissue (N). q values are shown and are colour-coded based on the level of significance. (G) Integrative genomics viewer (IGV) images showing enrichment of H3K27ac peaks around *ASCL2, SALL4* and *FZD10* genes using aggregate ChIP-Seq profiles of normal colon, adenoma and CRC tumours. (H) Violin plots showing mRNA expression levels for *ASCL2, SALL4* and *FZD10* in adenomas, the adenocarcinoma cohort used in this study (labelled as MDACC) and The Cancer Genome Atlas (TCGA) adenocarcinoma cohort. The reported p values were calculated using the *DESeq2*.[52] (I) List of enriched transcription factor (TF) motifs in CRC- or normal tissue-specific active enhancers. Motifs are identified using HOMER[27] on the basis of the shared H3K27ac peak in each group. ChIP-Seq, chromatin immunoprecipitation sequencing.

the proximity of key WNT signalling regulators such as ASCL2, SLL4, FZD10, CTNNB1 (β-catenin), AXIN2, LEF-1 and a subset of these correlated with their progressive increase in gene expression (figure 1G,H, online supplemental figure S3A–C and table S2). This suggests that the genes identified to harbour active enhancers or super enhancers near their vicinity or in regions interacting with the gene body/promoters are likely to contribute to the carcinogenic properties. Enhancers are epigenetic platforms for binding of various transcription factors (TFs), and motif enrichment analysis has suggested that specific classes of TFs such as forkhead (FOXA1, FOXA2 and FOXM1), ETS (ETV4, ERG and FLI1) and bZIP (ATF3 and AP-1) are over-represented in the tumour-specific active enhancers (figure 1I and online supplemental figure S3D). Importantly, homeobox

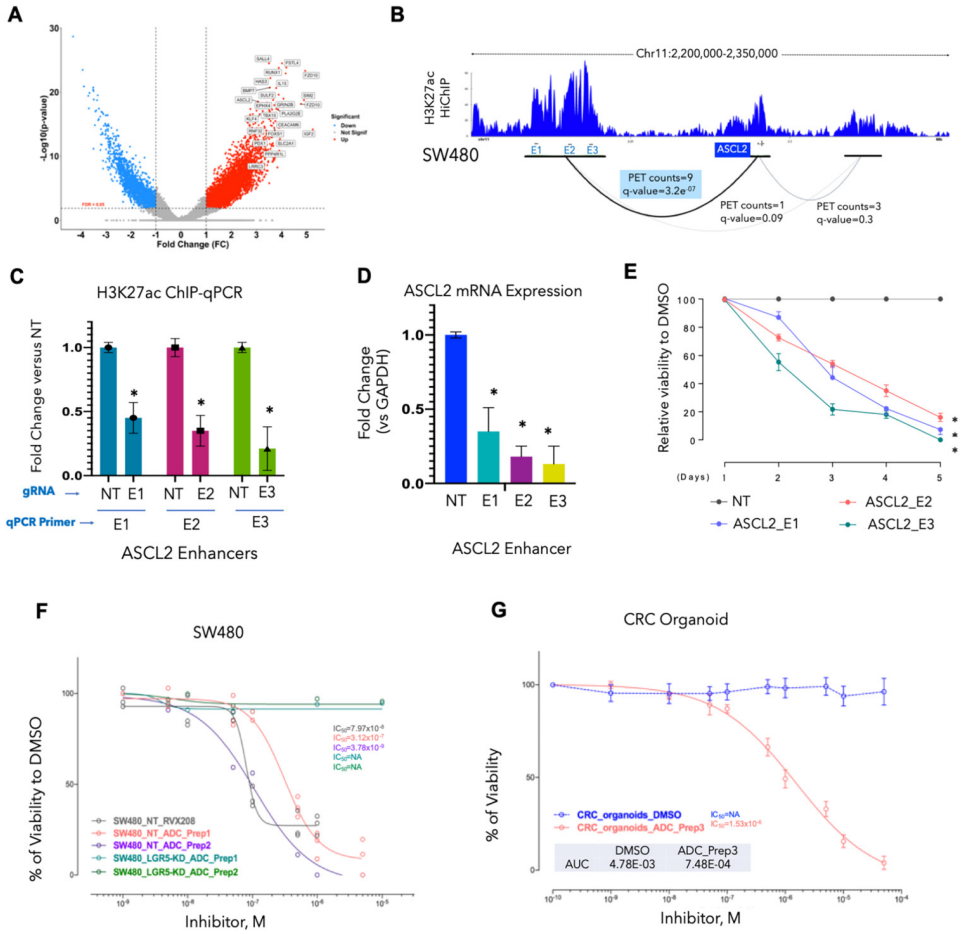

Figure 2 Inactivation of top tumour-specific enhancers leads to transcriptional downregulation and loss of cell proliferation. (A) Volcano plot showing top CRC-enriched typical enhancers ranked based on fold change and p value. Top de novo gained enhancers among tumour (n=33) as compared with adjacent normal (n=15) samples are annotated according to their associated genes. thresholds of log2FC>1 and FDR<0.05 are used to annotate de novo enhancer peaks. *ASCL2* and *FZD10* enhancers are among this subset of highly enriched regions. There are two top ranked enhancer peaks around Fzd10 gene. (B) Interaction map of active enhancers (E) with the gene promoter (P) around the *ASCL2* locus as determined in SW480 cell line by HiChIP. Interactions were observed in a super enhancer (E1–E3) region located ~70 kb upstream of *ASCL2* promoter (PET counts=9, q value=3.2e^{-07}). These regions are among the highly enriched tumour-specific enhancers and were present in multiple CRC cell lines (online supplemental figure S4A). (C) Bar graph showing relative enrichment of H3K27ac as derived from a ChIP-qPCR experiment on E1-E3 for *ASCL2* super-enhancer (B) in SW480 cells harbouring specific or non-targeting (NT) gRNAs to these enhancers. Y-axis represents fold change in intensity of H3K27ac signal for each enhancer in gRNA harbouring cell in comparison to the cells harbouring nt gRNA. *P<0.05. (D) Bar graph showing relative ASCL2 mRNA expression in E1-E3 gRNAs for *ASCL2* super enhancer harbouring SW480 cells in comparison to parental cells (ASCL2_NT). (E) Growth curve showing relative viability of SW480 cells harbouring E1–E3 for ASCL2 super enhancer in comparison to parental cell (ASCL2_NT) showing lower rates of proliferation in cells with *ASCL2*-inactivated enhancers. (F) Growth curves for LGR5-silenced SW480 cells (SW480$^{LGR5\text{-}KD}$) in comparison to the parental cells on treatment with increasing concentrations of two preparations of antibody-drug conjugate (ADC) with bromodomain inhibitor (RVX208) conjugated to LGR5 antibody (ADC-Prep1 and ADC-Prep2) and RVX-208 alone. Y-axis shows per cent viability of treated cells in comparison to control (DMSO) treated cells. (G) Growth curves for a patient-derived CRC organoid on treatment with LGR5-RVX208 conjugate (ADC). Y-axis shows per cent viability of treated cells in comparison to control (DMSO) treated cells. ChIP, chromatin immunoprecipitation; CRC, colorectal cancer; FDR, false discovery rate.

(NKX3.1), interferon regulatory factors (IRF1, IRF2), basic Helix-Loop-Helix (bHLH - NeuroG2, TCF4) and FOXO1 motifs were enriched in active enhancers that were lost during tumour progression (figure 1I and online supplemental figure S3D).

Inactivation of tumour-specific enhancers leads to the transcriptional and phenotypical switch

To test the functional role of some of the specifically activated tumour-specific enhancers, we first ranked the top differentially activated enhancers (figure 2A and online supplemental table S3; see Methods). We chose to functionally test some of the top enhancers from this list that were located in the vicinity of two WNT signalling genes: *ASCL2* and *FZD10*. *ASCL2* is a known driver of intestinal stem cell phenotype[19] and a predicted oncogene in CRCs[20] whereas, *FZD10* is a transmembrane protein that acts as a WNT receptor driving downstream signalling, which is a key signalling event in CRCs.[21] Moreover, established CRC cell lines harboured a significant percent of tumour-specific H3K27ac peaks (online supplemental figure S4A,B). We used dCas9-KRAB and specific gRNAs to suppress the activity of target enhancer loci in SW480 cells (online supplemental figure S4C), a well-characterised model with mutations in *APC*, *KRAS*, and *TP53*.[19] For ASCL2, we chose to focus on a distal super

enhancer that was present in the adenomas and adenocarcinomas, but not normal tissues (figures 2B and 1H, online supplemental figure S3A). HiChIP and 3C experiments confirmed the direct interaction of this super-enhancer with the ASCL2 gene promoter (figure 2B and online supplemental figure S4D). We noted that all three gRNAs targeting this distal super-enhancer region were able to suppress the H3K27ac signal in their respective target regions (figure 2C). These gRNAs also downregulated gene expression (figure 2D) and downstream proliferation of SW480 cells, suggesting that the distal super-enhancer acts as a functional driver event in this cell line (figure 2E). For the FZD10 locus, we noted that gRNAs targeting E1, E5 and E6 regions reduced the H3K27ac signal, which was consistent with the observations from HiChIP experiments showing the interaction of these enhancers with the promoter of this gene (online supplemental figure S4E,F). Epigenetic suppression of these enhancers also downregulated gene expression (online supplemental figure S4F) and decreased cell proliferation (online supplemental figure S4H), suggesting multienhancer regulation of FZD10 transcription and the contribution of this locus to the proliferative properties of CRC cells.

Although these studies provide evidence for the functionality of individual enhancers, a holistic approach would be to block many such enhancers using BRDi, which are being actively tested in clinical trials in solid tumours. Since ASCL2 and WNT pathways have established roles in regulating stem cell function in both normal and cancer tissues,[19–21] we asked whether targeting enhancer-blocking agents to stem cells, using the leucine rich repeat containing G protein-coupled receptor 5 (LGR5) antibody, would result in suppressing the growth of the cells. Hence, we synthesised an antibody-drug conjugate (ADC) by using LGR5 antibody and the RVX208 which is a BRDi in phase 3 trials for cardiovascular indications.[22] Indeed, LGR5-RVX208 (online supplemental figure S5A) ADCs specifically blocked the growth of SW480 cells or patient-derived human colon organoids in an LGR5 expression–dependent fashion (figure 2F,G and online supplemental figure S5B–E). These studies established that some of the activated enhancers in tumours may play functional roles in imparting protumourigenic properties to CRC.

Combination of MEK and BRDi reduces tumour growth in a subset of patient-derived xenografts

Treatment of four different patient-derived xenograft (PDX) models (C1138, F3053, F3008 and B8131) with BRDi (iBET-151) caused strong tumour reduction in one model but showed no significant difference in three of four models, suggesting a context-dependent impact of enhancer blockade (figure 3A,B). Since chromatin aberrations are believed to be a permissive event for activation of pro-tumourigenic transcriptional signature on oncogenic signalling, we reasoned that blockade of enhancers may be more effective in combination with inhibition of key oncogenic driver signalling pathways. We noted that a number of upstream regulators of the MEK pathway, including *EGFR*, *NRAS*, *KRAS*, *FGFR3*, *MAPK3K1*, *MAPK11*, *MAPK12, MAP3K20*, *MAP3K10*, *AKT2*, *IRS2*, *FGF1, FGF3*, *FGF19* and *FGF21*, gained enhancers in colorectal tumours in comparison to adjacent normal tissues or adenomas (online supplemental figure S6A). Therefore, we analysed whether enhancer-blocking BRDi may synergize with MEKi, which are actively being used in CRC clinical trials, to enhance therapeutic efficacy. Indeed, the treatment of four different PDX models (C1138, F3053, F3008 and B8131) showed significant synergy between MEKi (trametinib or binimetinib) and BRDi in three of these four models (figure 3A,B and online supplemental figure S6B). Although monotherapy with MEKi showed moderate activity on tumour growth in all of the models, significant tumour regression was noted in B8131, and two models (F3052 and 3008) showed slower growth in combinatorial treatment with BRDi.

To understand the epigenetic mechanism behind differential responses to BRDi and the combination therapy with MEKi, we performed ChIP-Seq for H3K27ac in Vehicle, BRDi (iBET-151), MEKi (Trametinib) and BRDi plus MEKi (iBET-151 plus Trametinib) treated tumours for C1138 and B8131 which exhibited poor or strong responses to the combination therapy, respectively. We noted that while MEKi had a modest impact on intensity of H3K27ac enhancer peaks, BRDi as well combination highly reduced total number of H3K27ac peaks as well as average intensity in comparison to control sample (figure 3C and online supplemental figure S6C). Comparison of H3K27ac peaks between C1138 and B8131 tumours showed the enrichment of various growth signalling pathways, including canonical MAPK pathway, in uniquely enriched peaks in C1138 in comparison to B8131 (figure 3D, online supplemental figure S6D and table S4). Consistently, reverse protein phase array (RPPA) data from the PDX models showed increase in GRB2, S6 kinase and IGFBP2 expression in C1138 tumours in comparison to B8131 (figure 3E). Pathway analysis of gene targets of H3K27ac peaks that were depleted on BRDi treatment in B8131 (responder), but not in C1138 (non-responder), shows multiple pathways implicated in resistance to MEKi such as mTOR, WNT and insulin signalling (figure 3F and online supplemental table S4).[23] These included important regulators of these pathways such as GRB2, AKT2, SMAD7, FZD5, SMAD3, RAC1, 4EBP1, IRS2 and MAP3K10 (figure 3G and online supplemental figure S6E). Overall, these data highlight the heterogeneous responses of various PDX models to enhancer blockade and suggest that pre-existing enhancer states may underlie responses to monotherapy of BRDi and MEKi/BRDi combination therapy.

Distinct enhancer-driven EPIgenome-based Classification clusters of CRC

As exemplified by the MEKi+BRDi combination treatment results, all CRC tumours do not respond to the blanket therapies equally. This motivated us to perform molecular characterisation of CRC tumours based on their epigenomic content, which can be potentially useful for patient stratification and subsequent assignment of each subtype to particular combination treatment with epigenetic compounds.

We classified adenomas and adenocarcinomas by using a consensus non-negative matrix factorisation (NMF)-based clustering method that uses the enriched H3K27ac peaks. Based on the cophenetic and dispersion scores, we identified four distinct clusters of tumours (figure 4A, online supplemental figure S7A,B and table S5), hereafter referred to as EPIgenome-based classification (EpiC) clusters: EpiC1, EpiC2, EpiC3 and EpiC4. The average intensity of enhancer peaks within these clusters varied such that EpiC2 and EpiC4 enhancers had significantly higher peaks than the other two clusters had (online supplemental figure S7C,D). EpiC3 clusters had the least overall peak intensity (online supplemental figure S7C,D). The distribution of H3K27ac peaks in regard to the gene body was similar across EpiC clusters (online supplemental figure S7E). EpiC clusters also did not associate with any known batches (online supplemental figure S8A). To interrogate the contribution of different cell types to EpiC classification, we overlapped EpiC-specific enhancers with those from 91 different cell types/datasets from ENCODE project (online supplemental figure S8B–G).[24] This analysis showed significant overlap

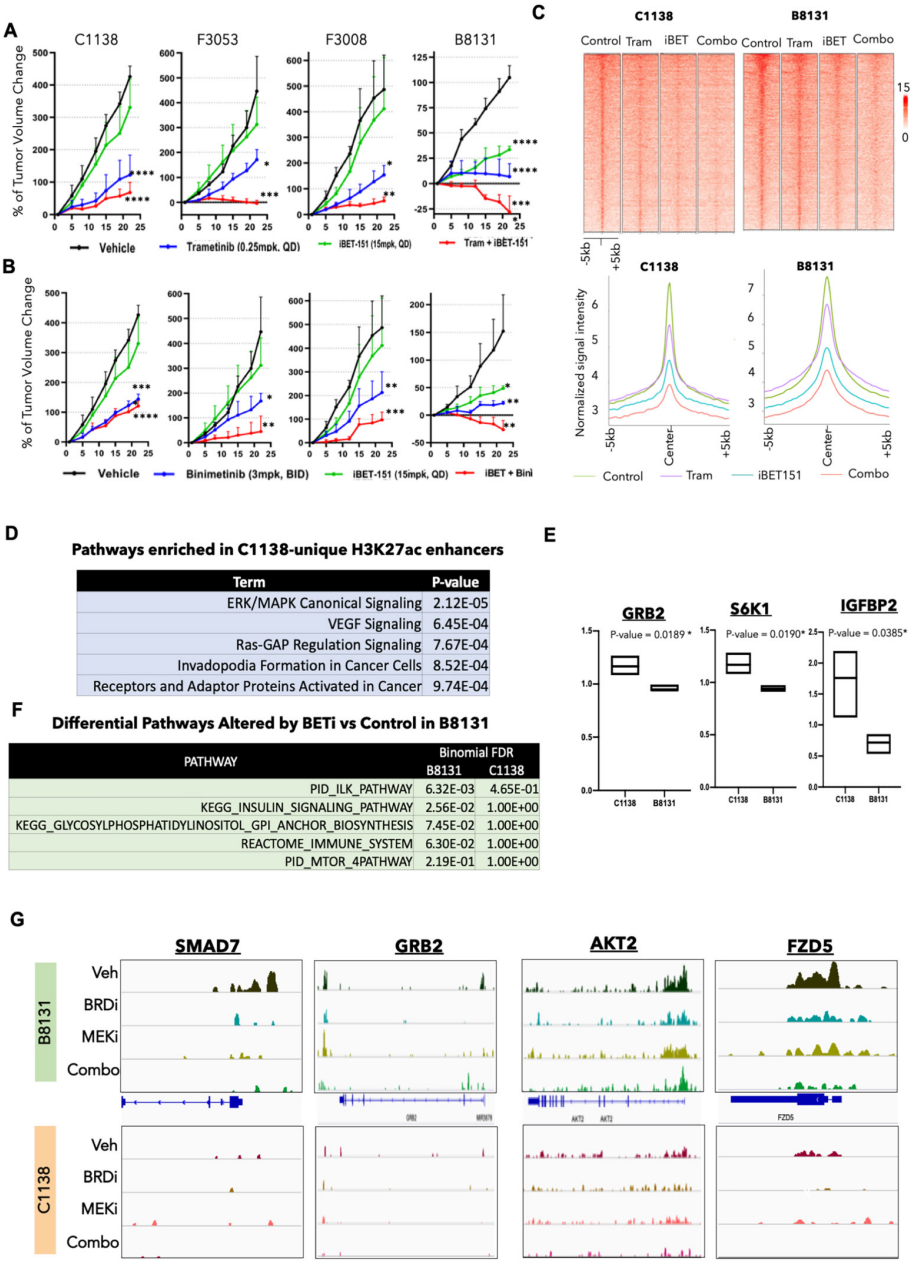

Figure 3 BRDi plus MEKi shows differential responses in different PDX models. (A) Tumour volume curves for C1138, F3053, F3008 and B8131 on treatment with MEK inhibitors (trametinib), BRD inhibitor (iBET151), and a combination of MEK and BRD inhibitors (trametinib +i-BET151) along with the control vehicle group (n=3–5 for each arm). P values represent pairwise *t* test comparison between the experimental arm to vehicle treatment. *P<0.05; **p<0.01; ***p<0.001; ****p<0.0001. Please refer to online supplemental figure S6B for all pair-wise comparisons of the p values. (B) Tumour volume curves for C1138, F3053, F3008, and B8131 on treatment with MEK inhibitor (binimetinib), BRD inhibitor (iBET151), and a combination of MEK and BRD inhibitors (binimetinib + iBET151) along with the control vehicle group (n=3–5 for each arm). P values represent pairwise t-test comparison between the experimental arm to vehicle treatment. *P<0.05; **p<0.01; ***p<0.001; ****p<0.0001. Please refer to online supplemental figure S6B for all pairwise comparisons of the p values. (C) Heatmap (top panel) and average intensity plot (bottom panel) for H3K27ac peaks in vehicle, trametinib, iBET-151 and combination (iBET-151 plus trametinib) treated PDXs, B8131 (Responder) and C1138 (non-responder). (D) Elsevier pathways (identified by Enricher) enriched in gene targets of H3K27ac peaks unique to C1138 vs B8131 PDXs. (E) Box plots showing protein expression (RPPA) of GRB2, S6K1 and IGFBP2 enriched in C1138 vs B8131 PDXs. (F) Differential pathways between those enriched in gene targets of lost H3K27ac-peaks in iBET-151 versus control treated B8131 and C1138. (G) IGV snapshots of H3K27ac peaks around *SMAD7, GRB2, AKT2* and *FZD5* in vehicle, trametinib, iBET-151 and combination (iBET-151 plus trametinib) treated B8131 and C1138. BRDi, bromodomain inhibitors; IGV, Integrative Genomics Viewer; PDX, patient-derived xenograft.

of EpiC1-specific enhancers with those from immune cells (online supplemental figure S8B–G), whereas enhancers unique to other three EpiCs only showed modest overlap to those from other non-colon cell types (online supplemental figure S8B, D–G) suggesting while EpiC1 classification may be convoluted from infiltration of immune cells, other EpiCs are likely derived from tumour-cell intrinsic enhancers.

Previously, four CMSs had been defined on the basis of transcriptomic signatures of more than four thousand CRC samples[3] as the CMS1 (MSI immune subtype), CMS2

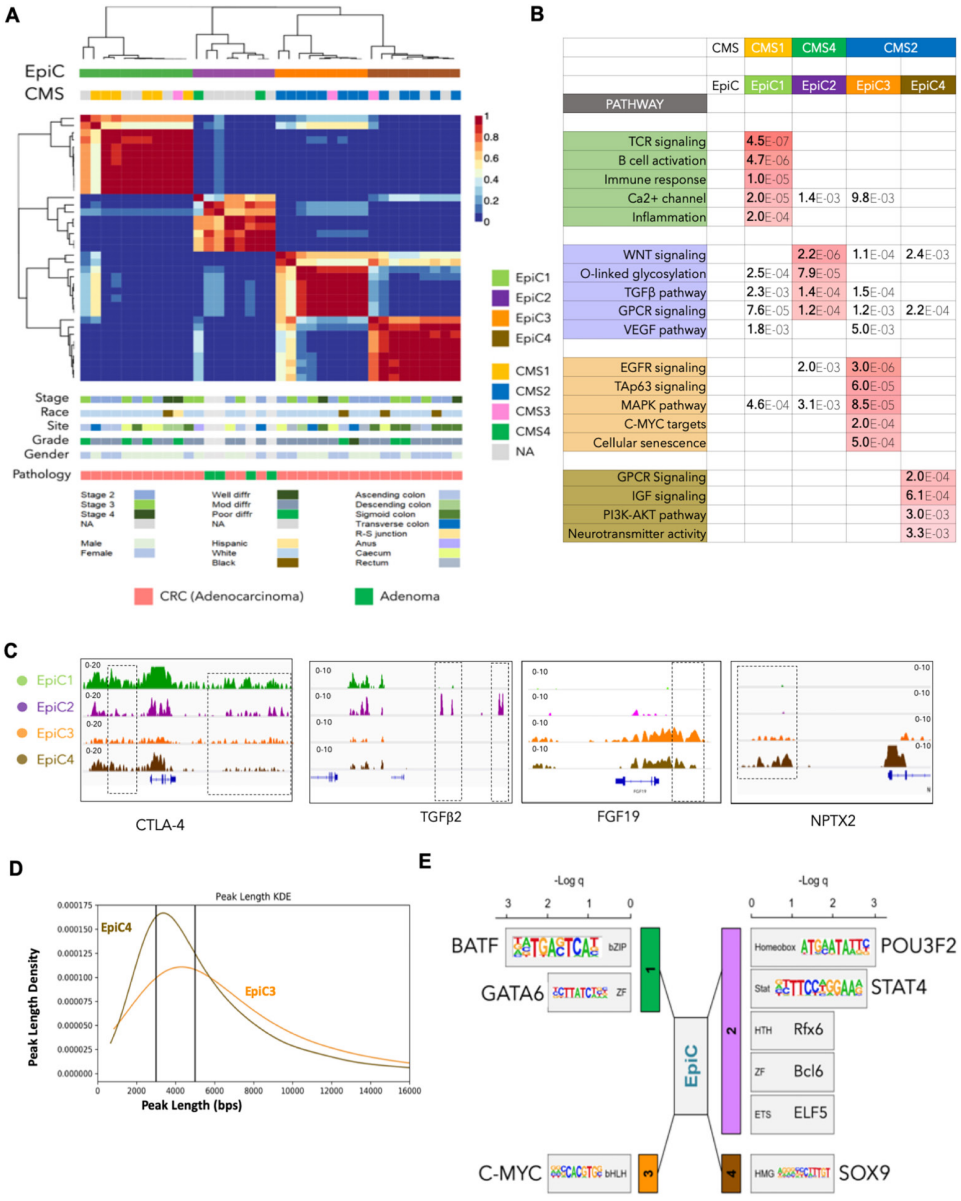

Figure 4 Reclassification of colorectal cancer (CRC) tumours based on their global enhancer distribution leads to identification of enhancer-based subtypes. (A) Non-negative matrix factorisation (NMF) clustering of CRC adenocarcinoma (n=33) and adenoma (n=4) samples identified four EPIgenome-based classification (EpiC) clusters of CRC, shown in the colour-coded matrix on the top panel. Consensus molecular subtype (CMS) classification of each tumour sample is identified by using a 498 gene–based random forest approach and is overlaid with the EpiC clusters. Clinical data corresponding to the tumour samples in each cluster, including tumour stage, site, pathological grade, race, and gender of the patients, are provided in the lower panels. (B) Table showing enriched major signalling pathways for genes targeted by EpiC-specific enhancers using GREAT.[17] False discovery rate (FDR) values are colour-coded. (C) IGV images showing enrichment of H3K27ac peaks around *CTLA4* for EpiC1, *TGFβR3* in EpiC2, *FGF19* in EpiC3 and *NPTX2* in EpiC4 using aggregate ChIP-Seq profiles of EPIC1, EpiC2, EpiC3 and EpiC4 group tumours. (D) KDE (kernel density estimate) plot with peak lengths (x-axis) and densities (y-axis) of EpiC3 and EpiC4-specific enhancers. peaks with length more than 5 kbs were annotated as broad whereas those with <3 kb in length were called as sharp. (E) Motif enrichment analysis for enhancers unique to different EpiC groups using HOMER.[27] ChIP-Seq, chromatin immunoprecipitation sequencing; IGV, Integrative Genomics Viewer; TGFβ, transforming growth factor-β.

(canonical subtype), CMS3 (metabolic subtype) and CMS4 (mesenchymal subtype). We classified the tumours used in our study into these CMSs, for which we had gene expression data, by using the CMS classifier,[25] and based on the corresponding trained model,[3] we computed their EpiC subtype. Interestingly, we determined that epigenomic clusters (EpiCs) significantly overlap their assigned CMSs (figure 4A). All of the samples classified as CMS1 (immune) subtype overlapped with the EpiC1 subtype. Although only two patients had been assigned to the CMS4 (mesenchymal) subtype, strikingly, all four adenoma samples along with these two patients clustered as the EpiC2 subtype. It has been shown that adenoma lesions have mesenchymal properties and may progress to adenocarcinoma due to aberrations in the Ras signalling pathway.[26] Moreover, consensus NMF clustering divided the canonical subtype or CMS2 into two novel subsets of epigenomic CRC clusters, EpiC3 and EpiC4 (figure 4A). Of note, the metabolic subtype or CMS3 is not detectable with the use of enhancer-based epigenomic clustering and is scattered in multiple subtypes.

Interestingly, pathway analysis based on the gene targets of enhancers (see the Methods section) that are specifically enriched in each EpiC subtype showed similarity to those known to be CMS-specific[3] (figure 4B). Enhancers specific to EpiC1, which overlaps significantly with CMS1, were in the proximity of genes regulating immune response, B-cell and T-cell activation and inflammation. EpiC2, which overlaps with CMS4 and interestingly contains all adenoma samples, regulates the transforming growth factor β (TGFβ), WNT and VEGF pathways (figure 4B). CMS2 CRC tumours were distributed into two epigenetic subtypes EpiC3 and EpiC4. EpiC3 enhancers enriched on targets of c-MYC, EGFR, MAPK and TAp63 signalling, whereas EpiC4 enhancers activated genes involved in GPCR, IGF, PI3K-AKT and neurotransmitter signalling (figure 4B and online supplemental table S6). Examples of important genes near the EpiC-specific enhancers are shown in figure 4C and online supplemental figure S9. We also noted that EpiC3 enhancers were more spread (or 'broad') in nature whereas EpiC4 enhancers were narrower in their width (or 'Sharp') (figure 4D). Systematic analysis of broad (>5 kb) and sharp (<3 kb) peaks (see the Methods section) showed enrichment of broad peaks in EpiC3 vs sharp peaks in EpiC4 enhancers figure 4D and online supplemental figure S9B) suggesting that likely two different epigenetic regulatory processes are responsible for establishment of the observed enhancer patterns in EpiC3 versus EpiC4 colorectal tumours.

To identify potential regulators of the EpiC-specific features, we performed motif analyses of enhancers specific to each EpiC subtype using HOMER.[27] Interestingly, distinct TF classes were enriched in each of the EpiC subtypes. bZIP (BATF) and ZF (GATA6) type TFs were enriched in EpiC1, and homeobox (BRN2 or POU3F2) and Stats (STAT4) were enriched in EpiC2; c-MYC (bHLH) was enriched in EpiC3, and HMGs (SOX9) were enriched in EpiC4 (figure 4E). Consistently, we noted that expression of TFs (except for POU3F2) was higher, specifically in the respective CMSs in The Cancer Genome Atlas (TCGA) samples that corresponded with EpiC subtypes (online supplemental figure S9C). Importantly, previous studies have implicated c-MYC,[28–31] GATA6,[32–34] SOX9[35–37] and STAT4[38 39] in CRC progression. BRN2/POU3F2 has oncogenic roles in melanoma[40 41] and BATF2, a BATF family member, has been implicated in CRC.[42] These data suggest that the potential origin of different EpiC subtypes may be due to the pioneering activity of TFs belonging to different classes of TF families.

Combinatorial treatments for EpiCs

The CMS classification is being tested as a prognostic indicator for use in targeted therapy in CRC. For example, the CMS1 and CMS4 subtype cell lines are more responsive to HSP90 inhibitor, whereas the CMS2 subtype shows more sensitivity to WNTi and EGFRi.[43 44] The CMS3 subtype is enriched in metabolic pathways and RAS mutations, but therapeutic vulnerabilities are unknown.[3]

Exploring the clinical implications of our findings, we used a panel of 11 signalling pathway inhibitors that are known to be involved in the CRC tumourigenesis and whose key regulators showed differential enhancer enrichments in their vicinity in different epigenomic subtypes of CRC. Therefore, we treated six CRC cell lines with the signalling pathway compounds along with a panel of 8 known epigenetic inhibitors to treat cell lines from different CMSs, previously annotated with use of a CMS classifier (online supplemental figure S10A,B–S13A,B).[43 44] We further analysed both IC_{50} and AUC indices to choose compounds with the best potency as well as the highest efficiency (figure 5A–C, online supplemental figure S10B, S13A). We used a combination of one signalling pathway inhibitor along with the most efficient epigenetic inhibitor according to the generated drug matrix in distinct CMSs. Based on the analysis of monotherapies, we tested combinations of BRDi + poly (ADP-ribose) polymerase inhibitor (PARPi) for CMS1/EpiC1, BRDi + epidermal growth factor receptor inhibitor (EGFRi) for CMS2/EpiC3-4 and BRDi + transforming growth factor β inhibitor (TGFβi) for CMS4/EpiC2 and found the combinations to perform better in reducing cell growth in vitro (figure 5D–F and online supplemental figure S13B and S14A. Importantly, we observed drastically enhanced activities of these combinations in the in vivo experiments carried out in nude mice, compared with the results of experiments using monotherapies (figure 5G–I).

Importantly, these combinatorial therapies demonstrated specific activity to the corresponding CMS/EpiC and had a minor impact on other CMS/EpiC subtypes. Specifically, BRDi (iBET-151, 15 mg/kg)+PARPi (Olaparib, 50 mg/kg) showed more significant impact on CMS1/EpiC1 cells than CMS2/EpiC3-4 or CMS4/EpiC2 did; similarly, BRDi (iBET-151, 15 mg/kg)+EGFRi (Gefitinib, 100 mg/kg) impacted CMS2/EpiC3-4 cells specifically and BRDi (iBET-151, 15 mg/kg)+TGFβi (SB431542, 10 mg/kg) reduced tumour growth of CMS4/EpiC2 cells specifically (figure 5G–I). Notably, we did not observe much loss in tumour weight on treatment with these drug combinations suggesting little or no side effects of these therapies (online supplemental figure S14B).

CMS2 can be divided into two epigenetic subgroups with clinical significance

To determine if the observed dichotomy of CMS2 tumours into EpiC3 and EpiC4 in our cohort expanded to a larger set of CRC samples, we examined the clustering of CMS2-designated TCGA tumours[45] based on the gene targets of EpiC3 and EpiC4 enhancers. NMF clustering of 115 CMS2 tumours (see the Methods section) identified three clusters (online supplemental figure S15A and table S7): Clusters 1, 2 and 3. Overlap of EpiC4 enhancer target genes with Cluster2-specific genes showed enrichment of EpiC4-specific pathways such as GPCR, PI3K pathway and NCAM mediated neurotransmitter signalling (including NPTX2—a differentially expressed gene between EpiC3 and EpiC4) (online supplemental figure S15B–D). Overlap of EpiC3 enhancer target genes with Cluster3-specific genes showed enrichment of EpiC3-specific pathways such as EGFR signalling, MAPK, and c-MYC targets (figure 6A and online supplemental figure S15B,C). On the contrary, EpiC3-target genes overlap with Cluster3-specific genes or EpiC4-target genes overlap with Cluster2-specific genes did not enrich in any pathways specific for EpiC3 or EpiC4 (online supplemental figure S15C). Cluster 1-specific genes were mostly enriched in immune pathways suggesting likely separation due to low tumour content (online supplemental figure S15C). Therefore, we designated Cluster2 (n=37) as 'EpiC4-like' and Cluster3 (n=63) as 'EpiC3-like'. Importantly, EpiC3-like tumours showed poorer survival in comparison to EpiC4-like tumours (figure 6B and online supplemental figure S15D), thus providing clinical significance for enhancer-based classification of CRC tumours.

To further enhance the clinical significance of EpIC subgroups, we investigated if EpiC3 versus EpiC4 epigenomic patterns may impart specific therapeutic strategies in these subgroups because they both are categorised within the same transcriptomic group of CMS2. To exploit the combination strategy of BRDi with specific pathway inhibitors in these EpiC subgroups, we examined the RPPA data between EpiC3-like and EpiC4-like TCGA patients. We noted loss of PTEN and concomitant increase of mammalian target of rapamycin (mTOR) targets, 4EBP1 (pT70) and pS6 kinase, in

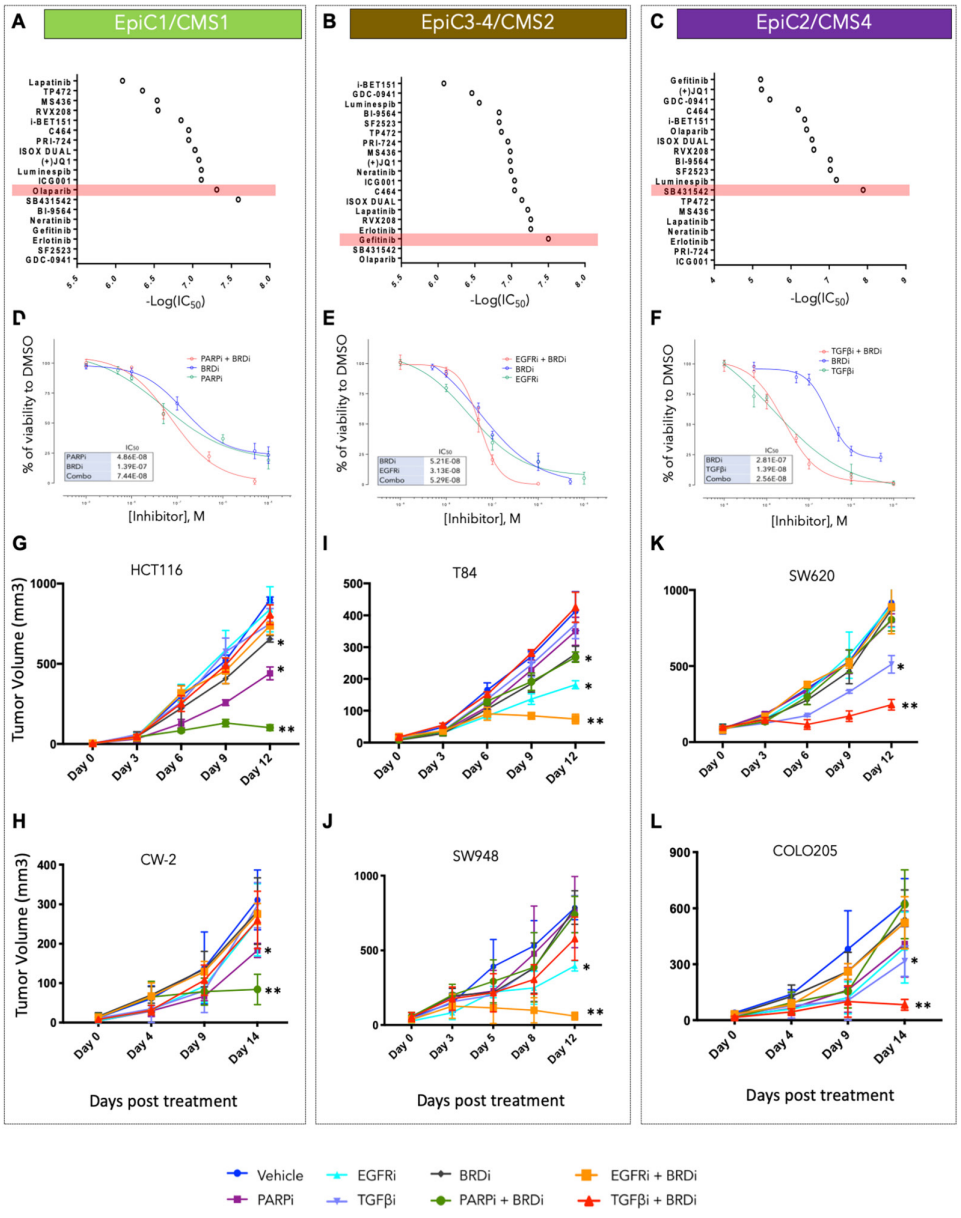

Figure 5 Correlation between CRC molecular subtypes and EpiCs can predict combinatorial treatments with high clinical significance. (A–C) Summary of IC_{50} values for 19 small molecule inhibitors (Y-axis) in cell lines with similar expression features to CMS1/EpiC1 (HCT116 or SW480) (A), CMS2/EpiC3 or EpiC4 (T84) (B), and CMS4/EpiC2 (SW620) (C). -Log(IC_{50}) values are demonstrated on X-axis for each of the compounds. Drugs with higher -Log(IC_{50}) are highlighted and were further used in combinatorial experiments. (D–F) Growth curves showing responses of CMS-specific CRC cell lines for the drug combinations identified based on the IC_{50} and AUC indices (panels A–C and Figures S8-S11): CMS1 lines with PARPi (olaparib) +BRDi (iBET-151) (D), CMS2 with EGFRi (gefitinib) +BRDi (RVX-208) (E), and CMS4 with TGFβi (SB431542) +BRDi (ISOX-DUAL) (F). (G–L) Tumour volume curves for xenografts in nude mice generated from transplantation of EpiC1/CMS1 (G–H), EpiC3-4/CMS2 (I–J), and EpiC2/CMS4 (K–L) cell lines on treatment with inhibitors of EGFR (gefitinib, 100 mg/kg), PARP (olaparib, 50 mg/kg), TGF-β (SB431542, 10 mg/kg), BRDi (I-BET151, 15 mg/kg), or the combination of EGFRi +BRDi, the combination of PARPi +BRDi, and the combination of TGF-βi+BRDi along with the control vehicle group. Mice were treated every other day. best treatment response was observed in the PARPi +BRDi combination in EpiC1/CMS1, EGFRi +BRDi combination in EpiC3-4/CMS2, and TGF-βi+BRDi combination in EpiC2/CMS4 lines. *P<0.05, **p<0.01. CMS, consensus molecular subtypes; CRC, colorectal cancer; BRDi, bromodomain inhibitors; EpiCs, EPIgenome-based Classification; TGF-β, transforming growth factor β.

EpiC3-like samples (figure 6C). On the other hand, EpiC4-like samples displayed increased levels of c-KIT proto-oncogene, receptor tyrosine kinase (c-KIT) and SRC proto-oncogene, non-receptor tyrosine kinase (SRC) phosphorylation (figure 6C). Based on this result and in line with the theme from previous results, we hypothesised that EpiC3-like tumour cells may be sensitive to mTOR inhibitors plus BRDi whereas EpiC4 group may be vulnerable to a combination of KIT/SRC inhibitors plus BRDi. For the functional analyses, we categorised previously CMS2-designated cell lines[43 44 46 47] into EpiC3 (SW948 and SW480) and EpiC4 (SW403 andT84) groups based on NPTX2 enhancer pattern and gene expression (a feature of EpiC4 subgroup, (online supplemental figure S15E) as well as RPPA data (online supplemental figure S15F,G). We then tested the sensitivity of the xenograft tumours from these cell lines to aforementioned combination therapy. Indeed, we found that combination of iBET-151 with

A

EpiC3-like (Cluster 3)

PATHWAY	FDR
Matrix mettaloproteinases	1.52E-04
ErbB signaling	1.14E-03
MAPK Signaling	1.36E-02
C-MYC targets	1.73E-02
EGFR	2.16E-02

EpiC4-like (Cluster 2)

PATHWAY	FDR
Epithelial-to-Mesenchymal Transition	6.04E-04
NCAM1 Interactions	7.03E-04
PI3K-AKT Pathway	5.17E-03
Axon guidance	5.98E-03
GPCR Signaling	3.14E-02

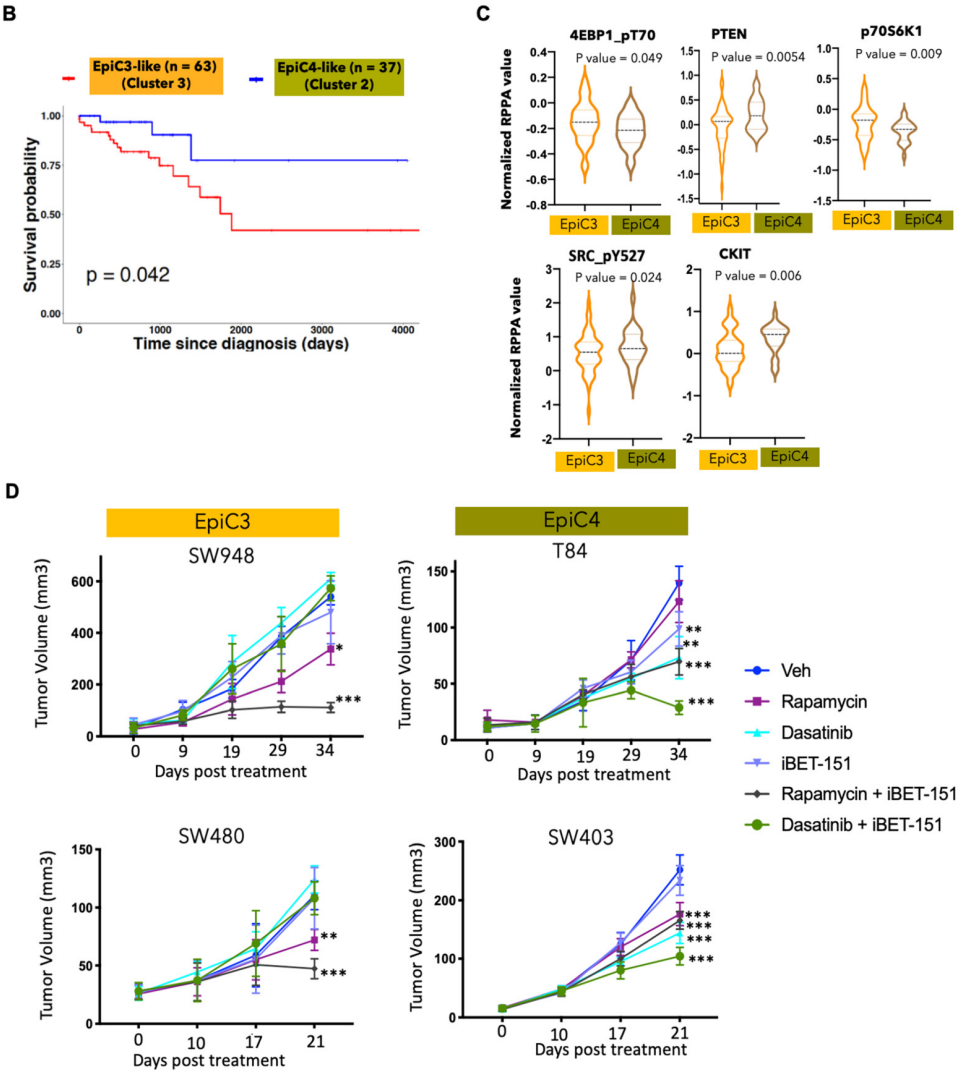

Figure 6 Functional and clinical significance of EpiC3 and EpiC4 classification. (A) Kaplan-Meier plot of survival of CMS2 samples in the TCGA, comparing EpiC4-like patients (n=37) and EpiC3-like patients (n=63). The log-rank (Mantel-Cox) p value is shown for the difference in survival. (B) Pathway analysis for genes in clusters 2 and 3 from NMF clustering (see online supplemental figure S9) of 115 CMS2 TCGA CRC tumours that overlap with EpiC3 and EpiC4-unique genes (LogFC >0.5 and p<0.05). based on the pathway enrichment, cluster two was annotated as 'EpiC4-like' whereas cluster three was annotated as 'EpiC3-like'. (C) Violin plots showing protein expression of 4EBP1_pT70, PTEN, p70S6K1, SRC_pY527 and cKit in EpiC3-like or EpIC4-like TCGA samples. (F) Tumour volume curves for xenografts in nude mice generated from transplantation of EpiC3 (left panels, SW948 and SW480) or EpiC4 (right panels, T84 and SW-403) cell lines on treatment with inhibitors of mTOR (rapamycin, 4 mg/kg), SRC/KIT (dasatinib, 30 mg/kg), BRDi (iBET-151, 15 mg/kg), or the combination of rapamycin + iBET-151 or the combination of dasatinib + iBET-151 or the control vehicle group. Mice were treated every other day. *P<0.05, **p<0.01, ***p<0.001. BRDi, bromodomain inhibitors; CMS, consensus molecular subtype; EpiC, EPIgenome-based Classification; NMF, negative matrix factorisation.

rapamycin (mTOR inhibitor) was able to suppress growth of xenograft tumours from EpiC3 cell lines whereas iBET-151 and Dasatinib (SRC/KIT inhibitor) combination was specifically highly effective in EpiC4 xenografts (figure 6D). Overall, these data provide specific therapeutic strategies for patients harbouring specific epigenomic signature.

DISCUSSION

Our study provides the most comprehensive data on basic epigenetic elements, in line with definitions from Roadmap/ENCODE, for human CRC, premalignant adenomas, widely used cell lines and normal crypts/tissues. Importantly, these tissues/cell lines have associated genomic, transcriptomic, drug-response and

clinical datasets available. Thus, these collective epigenomic maps elucidate the epigenomic makeup of CRC and are an essential resource, along with the previous datasets,[10–13] for the community to generate hypotheses regarding the roles of the epigenome in CRC progression. Based on this comprehensive resource, our unbiased chromatin state analyses identified the H3K27ac marked active enhancers are the most discriminatory epigenetic elements between the various histopathological stages of CRCs. Consistent with this, the number of enhancer peaks that differentiate adenomas, normal tissues and tumours is very high, suggesting that enhancer activation is likely a major epigenetic aberration in CRC. We suggest that enhancer aberrations are a critical component of a permissive chromatin environment in cancer cells that allow oncogenic events/pathways to drive excessive tumour growth. In addition to the active enhancer state, we also noted the heterochromatin state (H3K9me3) to differentiate between tumours and normal tissues. This will need to be further examined for causative effects.

We identified superenhancers surrounding *ASCL2* and *FZD10* to be necessary for CRC cell growth in vitro (figure 2 and online supplemental figure S4). This is interesting in that it provides evidence for enhancer/SE as being targets for therapeutics in the future, potentially with the evolution of CRISPR-based therapies. It is also imaginable that eRNAs made from such superenhancers may be targets for RNA-targeted therapeutics such as antisense oligonucleotides.[48] The advances in 3D epigenome studies, such as our HiChIP data, also suggest that one enhancer may target many genes and hence could prove to be a better therapeutic target than the presumed gene target itself. We found over >30000 such enhancers to be uniquely activated in colorectal adenocarcinomas. Future studies will be needed to identify functional enhancers such as those surrounding *ASCL2* and *FZD10*.

Most importantly, our work identifies heterogeneity in enhancer patterns between CRC patients and for the first time identifies epigenomic subtypes of CRC. We demonstrate that the EpiC subtypes correlate highly with the expression phenotype (CMS), in line with previous observations made in the pan-cancer TCGA assay for transposase-accessible chromatin using sequencing (ATAC-seq) study,[49] except that the CMS2 subtype was bifurcated into two distinct EpiC subtypes, EpiC3 and EpiC4. How these EpiC-specific enhancer patterns are setup and how they cooperate with genetic events for the transformation of normal cells into cancers with unique transcriptional signatures need to be studied in the future. This is an interesting observation since we hypothesise that EpiC3 is likely driven by a c-MYC-regulated transcriptional programme, whereas EpiC4 is driven by SOX9. Importantly, EpiC4 showed activation of enhancers around important neuronal genes (figure 3C and online supplemental figure S8), such as *NPTX2*,[50] which could be either due to neural invasion in this category of tumours[51] or epigenetic derepression of neuronal features. We suggest that inhibitors that target the c-MYC programme could be more useful in EpiC3 subtypes, whereas SOX9 may be a target in EpiC4 subtypes. Importantly, the two TCGA subsets with EpiC3 and EpiC4 like features showed significant difference in survival, hence providing a clinical significance of this bifurcation of the CMS2 subtype.

Finally, our data suggest that combination of BRDi as an umbrella approach for blockade permissive enhancer states along with specific driver signalling pathway inhibitors could be used in defined patient CRC populations, hence providing a paradigm for epigenome-focused personalised therapeutic strategy. BRDi combined well with PARP inhibitors for EpiC1, TGFβ inhibitors for EpiC2, mTOR inhibitors for EpiC3, and SRC/kit inhibitors for EpiC4. This is an important observation as it suggests patient stratification based on enhancer signatures as well as the use of epigenetic therapy in a patient-centric manner.

Author affiliations
[1]Department of Genomic Medicine, University of Texas MD Anderson Cancer Center, Houston, Texas, USA
[2]Broad Institute of MIT and Harvard, Cambridge, Massachussetts, USA
[3]Graduate Program in Quantitative and Computational Biosciences, Baylor College of Medicine, Houston, Texas, USA
[4]Department of GI Medical Oncology, University of Texas MD Anderson Cancer Center, Houston, Texas, USA
[5]MD Anderson Cancer Center UTHealth Graduate School of Biomedical Sciences, University of Texas MD Anderson Cancer Center, Houston, Texas, USA
[6]Center for Translational Cancer Research, University of Texas Health Science Center at Houston, Houston, Texas, USA
[7]Department of Clinical Cancer Prevention, University of Texas MD Anderson Cancer Center, Houston, Texas, USA
[8]University of Chicago Medical Center, Chicago, Illinois, USA
[9]University of Pennsylvania Perelman School of Medicine, Philadelphia, Pennsylvania, USA

Twitter Ayush T Raman @aayushraman, Archit K Ghosh @ArchitGhosh1 and Mayinuer Maitituoheti @mahinur mattohti

Acknowledgements We thank Veena Kochat, Sharon Landers and Angela Bhalla for helpful discussions and suggestions.

Contributors EO conceived, conceptualised and designed the study, planned and carried out experiments, analysed data, prepared figures and wrote the manuscript. ATR conceptualised and designed the study, performed computational analysis, prepared figures and wrote the manuscript. AKS contributed to study design, carried out experiments, performed computational analysis, prepared figures and wrote the manuscript. AS performed PDX experiments. EA performed computational analysis for CMS2 classification. AKG performed the 3C experiments and edited the manuscript. JS performed peak length analysis. MT helped with informatics analysis. CT, SCC, MM, KT, ZJ, JSD, SG, HML, LR-U, KC, YL, HC, AA, EA, YJ, SJ provided technical help. JM, EV, KSC and SK contributed to study design and provided reagents. KR conceived, conceptualised and designed the study, performed experiments, evaluated data, made figures and wrote the manuscript. All the authors edited the manuscript.

Funding This work was supported by ACS research scholar award, CPRIT IIRA award (RP200390), a Career Development Award from MDACC GI SPORE to KR. We thank Integromics group, the Advanced Technology Genomics Core Facility (NCI Grant CA016672(ATGC), the Research Animal Support Facility, the Advanced Microscopy Core Facility (funded by NIH S10 RR029552), Functional Genomics Core (NCI Cancer Centre Support Grant (P30 CA016672) and MD Anderson Cancer Centre Clinical Core.

Competing interests None declared.

Patient consent for publication Not required.

Provenance and peer review Not commissioned; externally peer reviewed.

Data availability statement Data are available in a public, open access repository. ChIP-seq, RNA-seq and Hi-ChIP datasets that support the findings of this study have been deposited in the Gene Expression Omnibus (GEO) database with the accession codes as follows: GSE136889 [https://www.ncbi.nlm.nih.gov/geo/query/acc.cgi?acc=GSE136889], GSE88945 [https://www.ncbi.nlm.nih.gov/geo/query/acc.cgi?acc=GSE88945], GSE106500 [https://www.ncbi.nlm.nih.gov/geo/query/acc.cgi?acc=GSE106500] and GSE136044 [https://www.ncbi.nlm.nih.gov/geo/query/acc.cgi?acc=GSE136044].

ORCID iDs
Elias Orouji http://orcid.org/0000-0002-7413-1383
Ayush T Raman http://orcid.org/0000-0003-2872-2307
Emre Arslan http://orcid.org/0000-0001-7224-917X
Eduardo Vilar http://orcid.org/0000-0001-6404-3761
Kunal Rai http://orcid.org/0000-0003-2321-6894

REFERENCES

1 Strum WB. Colorectal adenomas. *N Engl J Med Overseas Ed* 2016;374:1065–75.
2 Fearon ER, Vogelstein B. A genetic model for colorectal tumorigenesis. *Cell* 1990;61:759–67.
3 Guinney J, Dienstmann R, Wang X, *et al*. The consensus molecular subtypes of colorectal cancer. *Nat Med* 2015;21:1350–6.
4 Haan JC, Labots M, Rausch C, *et al*. Genomic landscape of metastatic colorectal cancer. *Nat Commun* 2014;5:5457.
5 Cancer Genome Atlas Network. Comprehensive molecular characterization of human colon and rectal cancer. *Nature* 2012;487:330–7.
6 Yaeger R, Chatila WK, Lipsyc MD, *et al*. Clinical sequencing defines the genomic landscape of metastatic colorectal cancer. *Cancer Cell* 2018;33:125–36.
7 Lovén J, Hoke HA, Lin CY, *et al*. Selective inhibition of tumor oncogenes by disruption of super-enhancers. *Cell* 2013;153:320–34.
8 Rai K, Sarkar S, Broadbent TJ, *et al*. Dna demethylase activity maintains intestinal cells in an undifferentiated state following loss of APC. *Cell* 2010;142:930–42.
9 Tao Y, Kang B, Petkovich DA, *et al*. Aging-like spontaneous epigenetic silencing facilitates Wnt activation, stemness, and BrafV600E^{V600E}-Induced tumorigenesis. *Cancer Cell* 2019;35:315–28.
10 Akhtar-Zaidi B, Cowper-Sal-lari R, Corradin O, *et al*. Epigenomic enhancer profiling defines a signature of colon cancer. *Science* 2012;336:736–9.
11 Cohen AJ, Saiakhova A, Corradin O, *et al*. Hotspots of aberrant enhancer activity punctuate the colorectal cancer epigenome. *Nat Commun* 2017;8:14400.
12 Hung S, Saiakhova A, Faber ZJ, *et al*. Mismatch repair-signature mutations activate gene enhancers across human colorectal cancer epigenomes. *Elife* 2019;8. doi:10.7554/eLife.40760. [Epub ahead of print: 13 Feb 2019].
13 Johnstone SE, Reyes A, Qi Y, *et al*. Large-scale topological changes restrain malignant progression in colorectal cancer. *Cell* 2020;182:e23:1474–89.
14 Ernst J, Kellis M. ChromHMM: automating chromatin-state discovery and characterization. *Nat Methods* 2012;9:215–6.
15 Yen A, Kellis M. Systematic chromatin state comparison of epigenomes associated with diverse properties including sex and tissue type. *Nat Commun* 2015;6:7973.
16 Whyte WA, Orlando DA, Hnisz D, *et al*. Master transcription factors and mediator establish super-enhancers at key cell identity genes. *Cell* 2013;153:307–19.
17 McLean CY, Bristor D, Hiller M, *et al*. Great improves functional interpretation of cis-regulatory regions. *Nat Biotechnol* 2010;28:495–501.
18 Cao Q, Anyansi C, Hu X, *et al*. Reconstruction of enhancer-target networks in 935 samples of human primary cells, tissues and cell lines. *Nat Genet* 2017;49:1428–36.
19 Schuijers J, Junker JP, Mokry M, *et al*. Ascl2 acts as an R-spondin/Wnt-responsive switch to control stemness in intestinal crypts. *Cell Stem Cell* 2015;16:158–70.
20 Zhu R, Yang Y, Tian Y, *et al*. Ascl2 knockdown results in tumor growth arrest by miRNA-302b-related inhibition of colon cancer progenitor cells. *PLoS One* 2012;7:e32170.
21 Terasaki H, Saitoh T, Shiokawa K, *et al*. Frizzled-10, up-regulated in primary colorectal cancer, is a positive regulator of the WNT - beta-catenin - TCF signaling pathway. *Int J Mol Med* 2002;9:107–12.
22 Rout A, Sukhi A, Chaudhary R, *et al*. Investigational drugs in phase II clinical trials for acute coronary syndromes. *Expert Opin Investig Drugs* 2020;29:33–47.
23 Kun E, Tsang YTM, Ng CW, *et al*. Mek inhibitor resistance mechanisms and recent developments in combination trials. *Cancer Treat Rev* 2021;92:102137.
24 ENCODE Project Consortium, Moore JE, Purcaro MJ, *et al*. Expanded encyclopaedias of DNA elements in the human and mouse genomes. *Nature* 2020;583:699–710.
25 Eide PW, Bruun J, Lothe RA, *et al*. CMScaller: an R package for consensus molecular subtyping of colorectal cancer pre-clinical models. *Sci Rep* 2017;7:16618.
26 Chen X, Halberg RB, Burch RP, *et al*. Intestinal adenomagenesis involves core molecular signatures of the epithelial-mesenchymal transition. *J Mol Histol* 2008;39:283–94.
27 Heinz S, Benner C, Spann N, *et al*. Simple combinations of lineage-determining transcription factors prime cis-regulatory elements required for macrophage and B cell identities. *Mol Cell* 2010;38:576–89.
28 Lee KS, Kwak Y, Nam KH, *et al*. Favorable prognosis in colorectal cancer patients with co-expression of c-myc and ß-catenin. *BMC Cancer* 2016;16:730.
29 Smith DR, Goh HS. Overexpression of the c-myc proto-oncogene in colorectal carcinoma is associated with a reduced mortality that is abrogated by point mutation of the p53 tumor suppressor gene. *Clin Cancer Res* 1996;2:1049–53.
30 Erisman MD, Rothberg PG, Diehl RE, *et al*. Deregulation of c-myc gene expression in human colon carcinoma is not accompanied by amplification or rearrangement of the gene. *Mol Cell Biol* 1985;5:1969–76.
31 Rochlitz CF, Herrmann R, de Kant E. Overexpression and amplification of c-myc during progression of human colorectal cancer. *Oncology* 1996;53:448–54.
32 Belaguli NS, Aftab M, Rigi M, *et al*. Gata6 promotes colon cancer cell invasion by regulating urokinase plasminogen activator gene expression. *Neoplasia* 2010;12:856–IN1.
33 Whissell G, Montagni E, Martinelli P, *et al*. The transcription factor GATA6 enables self-renewal of colon adenoma stem cells by repressing BMP gene expression. *Nat Cell Biol* 2014;16:695–707.
34 Martinelli P, Carrillo-de Santa Pau E, Cox T, *et al*. Gata6 regulates EMT and tumour Dissemination, and is a marker of response to adjuvant chemotherapy in pancreatic cancer. *Gut* 2017;66:1665–76.
35 Prévostel C, Blache P. The dose-dependent effect of SOX9 and its incidence in colorectal cancer. *Eur J Cancer* 2017;86:150–7.
36 Prévostel C, Rammah-Bouazza C, Trauchessec H, *et al*. Sox9 is an atypical intestinal tumor suppressor controlling the oncogenic Wnt/ß-catenin signaling. *Oncotarget* 2016;7:82228–43.
37 Lu B, Fang Y, Xu J, *et al*. Analysis of SOX9 expression in colorectal cancer. *Am J Clin Pathol* 2008;130:897–904.
38 Cheng JM, Yao MR, Zhu Q, *et al*. Silencing of STAT4 gene inhibits cell proliferation and invasion of colorectal cancer cells. *J Biol Regul Homeost Agents* 2015;29:85–92.
39 Slattery ML, Lundgreen A, Kadlubar SA, *et al*. JAK/STAT/SOCS-signaling pathway and colon and rectal cancer. *Mol Carcinog* 2013;52:155–66.
40 Herbert K, Binet R, Lambert J-P, *et al*. Brn2 suppresses apoptosis, reprograms DNA damage repair, and is associated with a high somatic mutation burden in melanoma. *Genes Dev* 2019;33:310–32.
41 Simmons JL, Pierce CJ, Al-Ejeh F, *et al*. Mitf and BRN2 contribute to metastatic growth after dissemination of melanoma. *Sci Rep* 2017;7:10909.
42 Dai L, Cui X, Zhang X, *et al*. SARI inhibits angiogenesis and tumour growth of human colon cancer through directly targeting ceruloplasmin. *Nat Commun* 2016;7:11996.
43 Sveen A, Bruun J, Eide PW, *et al*. Colorectal cancer consensus molecular subtypes translated to preclinical models uncover potentially targetable cancer cell dependencies. *Clin Cancer Res* 2018;24:794–806.
44 Linnekamp JF, Hooff SRvan, Prasetyanti PR, *et al*. Consensus molecular subtypes of colorectal cancer are recapitulated in in vitro and in vivo models. *Cell Death Differ* 2018;25:616–33.
45 The Cancer Genome Atlas Network. Comprehensive molecular characterization of human colon and rectal cancer. *Nature* 2012;487:330–7.
46 Berg KCG, Eide PW, Eilertsen IA, *et al*. Multi-omics of 34 colorectal cancer cell lines - a resource for biomedical studies. *Mol Cancer* 2017;16:116.
47 Ronen J, Hayat S, Akalin A. Evaluation of colorectal cancer subtypes and cell lines using deep learning. *Life Sci Alliance* 2019;2:e201900517.
48 Khvorova A, Watts JK. The chemical evolution of oligonucleotide therapies of clinical utility. *Nat Biotechnol* 2017;35:238–48.
49 Corces MR, Granja JM, Shams S, *et al*. The chromatin accessibility landscape of primary human cancers. *Science* 2018;362:eaav1898.
50 Xu C, Tian G, Jiang C, *et al*. NPTX2 promotes colorectal cancer growth and liver metastasis by the activation of the canonical Wnt/β-catenin pathway via FZD6. *Cell Death Dis* 2019;10:217.
51 Amit M, Takahashi H, Dragomir MP, *et al*. Loss of p53 drives neuron reprogramming in head and neck cancer. *Nature* 2020;578:449–54.
52 Love MI, Huber W, Anders S. Moderated estimation of fold change and dispersion for RNA-Seq data with DESeq2. *Genome Biol* 2014;15:550.